Magnetic Resonance Imaging 55 (2019) 52–59

Contents lists available at ScienceDirect

Magnetic Resonance Imaging

journal homepage: www.elsevier.com/locate/mri

Original contribution

Whole-tumor histogram analysis of non-Gaussian distribution DWI parameters to differentiation of pancreatic neuroendocrine tumors from pancreatic ductal adenocarcinomas☆

Jiali Li[a], Lili Liang[b], Hao Yu[a], Yaqi Shen[a], Yao Hu[a], Daoyu Hu[a], Hao Tang[a], Zhen Li[a,*,1]

[a] Department of Radiology, Tongji Hospital, Tongji Medical College, Huazhong University of Science and Technology, Wuhan, China
[b] Department of Radiology, The first affiliated hospital of Nanyang Medical College, China

ARTICLE INFO

Keywords:
Pancreatic carcinoma
Neuroendocrine tumors
Magnetic resonance imaging
Normal distribution
Microcirculation

ABSTRACT

Purpose: To evaluate the utility of volumetric histogram analysis of monoexponential and non-Gaussian distribution DWI models for discriminating pancreatic ductal adenocarcinoma (PDAC) and neuroendocrine tumor (pNET).

Materials and methods: A total of 340 patients were retrospectively reviewed. Finally, 62 patients with histopathological confirmed PDAC (n = 42) and pNET (n = 20) were enrolled in the study. All the patients accepted magnetic resonance imaging (MRI) at 3 T (including multi-b value DWI, 0–1000 s/mm^2). Isotropic apparent diffusion coefficient (ADC), true molecular diffusion (Dt), perfusion-related diffusion (Dp), perfusion fraction (f), distributed diffusion coefficient (DDC) and alpha (α) were obtained from different DWI models. Then, mean value, median value, 10th and 90th percentiles were obtained from histogram analysis of each DWI parameter.

Results: Histogram metrics derived from ADC, Dp, f and DDC were significantly lower in PDAC than pNET group ($P < 0.05$). In contrast, histogram metrics derived from α were observed significantly higher in the PDAC than pNET group ($P < 0.05$). No significant difference was found in Dt ($P \geq 0.05$) between PDAC and pNET patients. Among all parameters, f-median had the highest diagnostic performance (AUC 0.91, cutoff value 0.188, sensitivity 97.62%, specificity 80%).

Conclusions: f-Median derived from IVIM DWI model may be potentially more valuable parameter than ADC, Dp, DDC and α for discriminating PDAC and pNET. Histogram analysis based on the entire tumor was an emerging and valuable tool.

1. Introduction

Pancreatic ductal adenocarcinomas (PDAC) and neuroendocrine tumors (pNET) are the first and second common pancreatic tumor respectively [1,2]. However, the treatment strategy and prognosis are completely different. For pNET patients, more aggressive surgery approach may not significantly improve overall survival and lead to higher complications when compared with partial pancreatectomy [3]. For example, both the enucleation involving removal of just the tumor and the pancreaticoduodenectomy can be used to treat pNET. But the pancreaticoduodenectomy had significant morbidity [4], such as long-term gastrointestinal motility disorders and endocrine and exocrine insufficiency, while the enucleation can spare otherwise normal pancreatic parenchyma [5]. Given the fact that pNETs had a relatively well prognosis and higher resectability in comparison with PDACs, it would be a key component to differentiate pNETs from PDACs using preoperative imaging in clinical [6,7].

Dynamic MRI or CT is most frequently used to differentiate PDAC

Abbreviations: IVIM, Intravoxel incoherent motion; ADC, Apparent diffusion coefficient; Dt, True molecular diffusion; f, Perfusion fraction; Dp, Perfusion-related diffusion; DDC, Distributed diffusion coefficient; AUC, Area under the curve; pNET, Pancreatic neuroendocrine neoplasm; PDAC, Pancreatic ductal adenocarcinoma; ROC, Receiver operating characteristic; ROI, Region of interest

☆ This research was supported by the National Natural Science Foundation of China (grant numbers 81771801, 81701657, 81501447 and 81571642), and the Fundamental Research Funds for the Central Universities (grant number 2017KFYXJJ126).

* Corresponding author at: Department of Radiology, Tongji Hospital, Tongji Medical College, Huazhong University of Science and Technology, No. 1095 Jiefang Avenue, Wuhan, Hubei 430030, China.
E-mail address: zhenli@hust.edu.cn (Z. Li).
[1] Will handle correspondence at all stages of refereeing and publication, also post-publication.

https://doi.org/10.1016/j.mri.2018.09.017
Received 21 May 2018; Received in revised form 11 September 2018; Accepted 16 September 2018

and pNET in clinical practice. The characterized imaging appearance of PADC is hypovascular, as opposed to the often hypervascular appearance of pNET [8]. However, the atypical enhancement pattern of PDAC and pNET is not uncommon due to the differences in tumor differentiation and necrosis, leading to great difficulty in distinguishing them [9]. What's more, the toxicity of contrast agents is likely to pose a threat to patients with impaired renal function [10,11]. Hence DWI may be an alternative sequence to differentiate PDACs and pNETs for patients with renal insufficiency.

DWI is a relatively mature noninvasive imaging modality [12], which could display functional information without contrast media. An isotropic apparent diffusion coefficient (ADC) was calculated through monoexponential DWI model, which has been utilized to differentiate pancreatic tumors [13]. However, previous studies have demonstrated that the monoexponential model cannot really reflect the state of water molecules in the lesion [14]. Intravoxel incoherent motion (IVIM) and stretched exponential DWI models are based on non-Gaussian distribution theory. The IVIM model could separate the effects of microcirculation perfusion from the water molecules diffusion [15]. Previous study has indicated that IVIM parameters appear more accurate than ADC in identifying pancreas tumors [16]. The stretched exponential model, recently elucidated by Bennett et al. [17], could simultaneously quantify the diffusion of water molecules and voxel heterogeneity [18,19]. According to the investigation, the stretched exponential model has not been applied to identify pancreatic tumors.

Additionally, considering the heterogeneity of pancreatic cancer and neuroendocrine tumors, volumetric histogram analysis may superiorly reflect the heterogeneity. Previous studies have used ADC histogram analysis to differentiate pancreatic tumors [20]. However, there are limited researches that using the histogram of non-Gaussian distribution DWI models to differentiate pancreatic tumors.

Therefore, the purpose of this paper is to evaluate the diagnostic performance of different DWI mathematical models for differentiating PDAC and pNET, by using the whole-tumor histogram analysis.

2. Materials and methods

2.1. Patients

This study has obtained the permission from the local institutional review board and informed consent was waived. After a review of radiology database for the period of June 2012 to July 2017, we identified 340 patients, who were suspected of pancreatic tumor and underwent MR examinations Including DW imaging. According to the following exclusion criteria, 278 patients were excluded from this study: (a) patients who have accepted treatment before surgery; (b) no pathological results or pathologically confirmed other pancreatic tumors; (c) without multiple b values DWI examination; (d) inadequate image quality. Finally, 62 patients including 42 PDACs and 20 pNETs were enrolled. A flowchart of the study population was presented in Fig. 1.

2.2. MRI technique

MR examinations were performed with patients in a supine position, using a 32-channel torso array coil at 3.0-T system (Discovery MR750; GE Healthcare, Milwaukee, WI). The routine abdominal protocols were carried out, including: (a) coronal SSFSE sequence (repetition time/echo time [TR/TE], 2195.7/6.8 ms; matrix, 256 × 256; FOV: 36–44 cm; slice thickness, 5 mm; slice number, 18); (b) axial T1-weighted image (repetition time/echo time [TR/TE], 5 ms/2.5 ms; matrix, 256 × 256; FOV: 36–44 cm; slice thickness, 3 mm; intersection gap, 0 mm); (c) axial respiratory-triggered T2-weighted image (repetition time/echo time [TR/TE], 7500/84 ms; matrix, 256 × 256; FOV:36–44 cm; slice thickness, 4 mm; intersection gap, 1 mm), and finally (d) multiple b values DWI image. For patients who need to take dynamic contrast enhanced (DCE) - MRI examination, the DWI was obtained before the injection of contrast agents. Among the patients included in this study, 23 patients underwent contrast enhanced examination (PDAC = 15, pNET = 8), and 39 patients did not (PDAC = 27, pNET = 12).

The DWI (matrix, 256 × 192; FOV: 36–44 cm; slice thickness, 4 mm; slice number, 17; intersection gap, 1 mm; bandwidth 250 KHz/pix; acquisition time, 4–5 min; acceleration factor 3) was performed in the cross-section by using respiratory-triggered single-shot echo-planar sequence, and b values (including 0, 50, 100, 200, 300, 400, 500, 600, 700, 800, 900, 1000 s/mm^2) were used in patients.

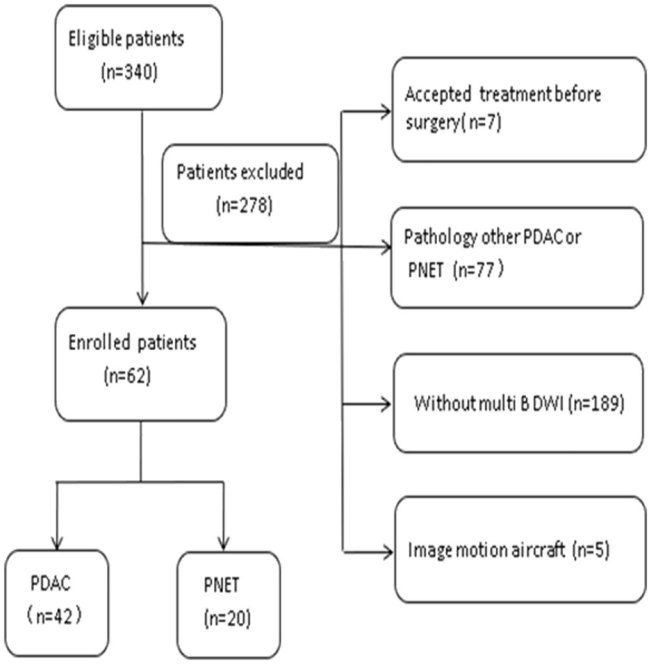

Fig. 1. Flowchart of the study population.

Table 1
Characteristics of patients with PDAC and pNET.

	PDAC	pNET	*P*
Number of patients	42	20	
Age, year	55(41–75)	48(39–65)	0.055
Sex			0.150
Man	17	12	
Woman	25	8	
Tumor size, cm	3.15(1.8–4.8)	2.91(2.1–4.55)	0.221
Location			0.897
Head	28	13	
Body or tail	14	7	

Data in parentheses are ranges.
PDAC = pancreatic ductal adenocarcinomas, pNET = pancreatic neuroendocrine tumors.

2.3. Image analysis

DICOM data of DWI was transferred from the picture archive and communication system (PACS) into a computer and processed with open source software Fire voxel (https://files.nyu.edu/hr18/public/projects.html). Two radiologists (6 and 14 years of imaging experience in abdominal MRI), unknowing the histopathologic results, reviewed all the MR images respectively. They manually drew the region of interest (ROI) along the edge of the lesion at each section referencing the axial T2-weighted image, while excluding areas of obvious cystic or necrosis. The ROI of each layer was fused automatically to obtain the whole tumor voxel information. Volumetric ADC map was constructed by

Table 2
The interobserver agreement between two radiologists of different histogram parameters.

Parameter	ICC	95% CI
ADC		
Mean	0.906	0.843–0.943
Median	0.921	0.869–0.952
10th percentile	0.948	0.914–0.969
90th percentile	0.956	0.927–0.974
Dt		
Mean	0.953	0.923–0.972
Median	0.896	0.827–0.937
10th percentile	0.875	0.792–0.925
90th percentile	0.981	0.969–0.989
Dp		
Mean	0.930	0.884–0.958
Median	0.971	0.952–0.983
10th percentile	0.850	0.751–0.910
90th percentile	0.931	0.886–0.959
f		
Mean	0.946	0.910–0.967
Median	0.978	0.964–0.987
10th percentile	0.942	0.904–0.965
90th percentile	0.992	0.986–0.995
DDC		
Mean	0.893	0.823–0.936
Median	0.864	0.774–0.918
10th percentile	0.880	0.801–0.928
90th percentile	0.973	0.956–0.984
α		
Mean	0.954	0.924–0.972
Median	0.985	0.975–0.991
10th percentile	0.966	0.943–0.979
90th percentile	0.945	0.909–0.967

ICC = intraclass correlation coefficient, CI = confidence intervals.

Table 3
Comparison of histogram parameters derived from DWI between PDAC and pNET.

Parameter	PDAC[a,b]	pNET[a,b]	*P*
ADC			
Mean	188.44 ± 23.39	224.2 ± 33.79	**0.000**
Median	173.96 ± 35.17	221.73 ± 32.06	**0.000**
10th percentile	106.68 ± 24.46	144.36 ± 32.79	**0.000**
90th percentile	257.88 ± 60.61	327.40 ± 98.15	**0.001**
Dt			
Mean	131.63 ± 21.25	142.1 ± 65.97	0.496
Median	123.66 ± 29.42	126.23 ± 71.68	0.879
10th percentile	98.40 ± 21.97	127.86 ± 101.78	0.215
90th percentile	185.74 ± 38.09	295.65 ± 242.85	0.058
Dp			
Mean	669.52 ± 137.68	815.5 ± 81.67	**0.000**
Median	485.26 ± 89.56	619.47 ± 69.05	**0.000**
10th percentile	207.32 ± 44.63	274.05 ± 53.33	**0.000**
90th percentile	792.39 ± 252.06	960.53 ± 85.29	**0.029**
F			
Mean	143.0.54 ± 35.82	252.16.11 ± 87.10	**0.000**
Median	133.32 ± 32.34	248.37 ± 99.77	**0.000**
10th percentile	36.90 ± 19.45	76.38 ± 42.35	**0.000**
90th percentile	298.88 ± 99.02	490.44 ± 183.74	**0.000**
DDC			
Mean	154.04 ± 33.08	203.85 ± 42.81	**0.000**
Median	153.82 ± 27.06	202.87 ± 33.81	**0.000**
10th percentile	105.19 ± 28.64	131.83 ± 38.23	**0.010**
90th percentile	215.86 ± 34.25	291.44 ± 98.32	**0.000**
α			
Mean	813.64 ± 53.70	733.52 ± 68.33	**0.000**
Median	836.61 ± 77.84	641.85 ± 179.96	**0.000**
10th percentile	602.91 ± 108.24	512.71 ± 109.16	**0.007**
90th percentile	975.35 ± 27.72	889.36 ± 93.70	**0.000**

Data are means ± standard deviations. Significant differences are in bold.
PDAC = pancreatic ductal adenocarcinomas, pNET = pancreatic neuroendocrine tumors.
[a] Units of 10^{-5} mm^2/s for ADC, Dt, Dp and DDC.
[b] Units of 10^{-3} mm^2/s for f and α in terms of mean, median, 10th and 90th percentile.

using a monoexponential fitting model:

$$S = S_0 exp(-b \times ADC)$$

where S represents the signal intensity in the presence of diffusion sensitization and S_0 represents the signal intensity in the absence of diffusion sensitization.

Tissue diffusivity (Dt), pseudo diffusivity (Dp) and perfusion fraction (f) were calculated, using IVIM biexponential Segmented Fit formula:

$$S = S_0 (f exp(-bD_p) + (1 - f)\, exp(-bD_t))$$

where f is linked to the intravascular component, Dp represents incoherent microcirculation, and Dt is the true diffusion coefficient that reflects random motion of intra- and intercellular water molecules.

Volumetric DDC and α map were constructed by using the stretched-exponential formula:

$$S = S_0 exp(-(b \times DDC)^{\alpha})$$

where α varies between 0 and 1 and represents the diffusion heterogeneity. A numerically high α value represents the low intravoxel diffusion heterogeneity. DDC value is related to the mean voxel diffusion rate.

Finally, the frequency table of each lesion was generated and exported. Then the histogram metric for every DWI parameter was calculated by IBM SPSS 23.0 (Chicago, IL), including: the mean, median, 10th and 90th percentiles.

2.4. Pathological evaluation

All pNET patients had their postoperative pathology reports, in which the tumor grade was reported. Tumor grade of pNET was reviewed and recorded by another reader unknowing the MRI information of patients.

2.5. Statistical analysis

All statistical analyses were conducted with MedCalc (MedCalc Software, Mariakerke, Belgium) and IBM SPSS 23.0 (Chicago, IL). $P < 0.05$ was deemed statistically significant.

Measurement consistency between two radiologists was checked by interclass correlation coefficient (ICC). The differences of mean age, gender, tumor diameter and tumor location between two groups were tested using the Mann–Whitney *U* test and the Chi-squared test, respectively. The Shapiro-Wilk test was applied to test normality of parameters ($P \geq 0.05$ is a normal distribution). The Student's *t*-test or Mann–Whitney U test was used for comparing the difference between two groups, depending on whether the data is distributed normally. Receiver operating characteristic (ROC) curve analysis was applied to obtain the optimal threshold, sensitivity, and specificity for differentiating PDACs and pNETs. The AUC difference was tested by the Z test.

3. Result

3.1. Patient and lesion characteristics

This study enrolled 62 patients confirmed by postoperative pathology (PDAC = 42, pNET = 20). We did not find significant

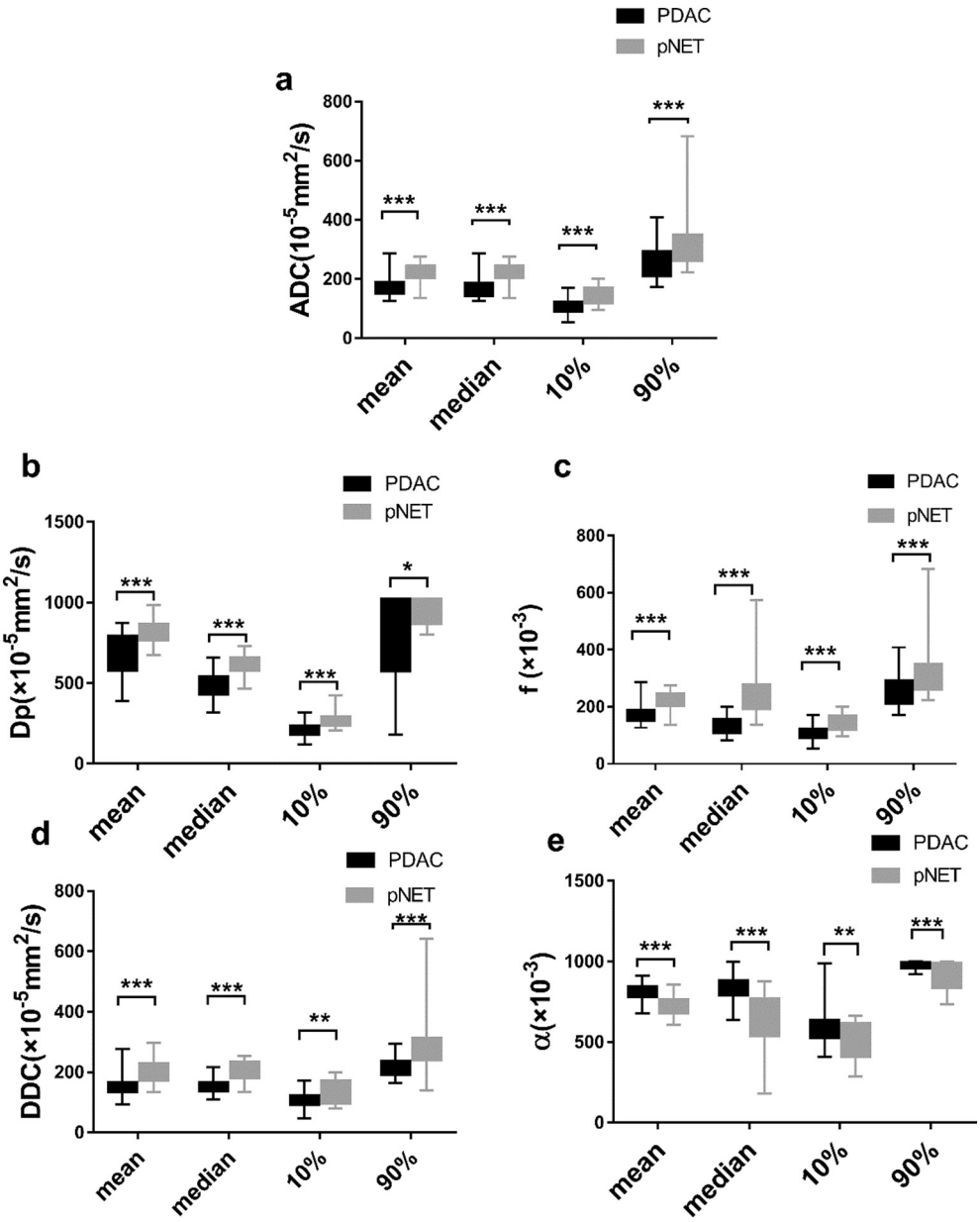

Fig. 2. Box-plot of the comparison of histogram parameters (mean, median, 10th, 90th percentiles) between PDAC and pNET in ADC (a), Dp (b), f (c), DDC (d) and α (e) values. *** $P < 0.001$; ** $P < 0.01$* $P < 0.05$.

difference in mean age, sex, tumor diameter and tumor location between pNET and PDAC ($P = 0.055$, 0.150, 0.221, 0.897, respectively) (Table 1).

3.2. Interobserver agreement

For all parameters, the interobserver agreement was excellent (ICC > 0.81) (Table 2). Thus, this study randomly chose a measurement value of one doctor for statistical analysis.

3.3. Histogram parameters comparison

The difference of histogram analysis of DWI parameters between PDAC and pNET groups was showed in Table 3. Histogram metrics derived from ADC, Dp, f and DDC were significantly lower in PDAC group than pNET groups ($P < 0.05$). In contrast, PDAC group had significantly higher histogram metrics derived from α than pNET group ($P < 0.05$). No significant difference was found in Dt value between PDAC and pNET groups ($P \geq 0.05$). The group-wise difference of significant parameters (ADC, Dp, f, DDC, and α) was showed in Box–plots (Fig. 2). Two sets of typical cases were shown in Figs. 3 and 4.

3.4. ROC analysis

During ROC analysis (Table 4), median had greater AUC than mean and other percentiles for every significant DWI parameter. f-Median had the highest diagnostic performance (AUC 0.91, cutoff value 0.188, sensitivity 97.62%, specificity 80%) than other medians (Dp-median, ADC-median, DDC-median, α-median), although none of these AUC differences reached statistical significance ($P \geq 0.05$) (Table 5). Fig. 5 exhibited the differences in diagnostic efficacy of parameters for differentiating PDAC and pNET.

3.5. Pathological result

Based on the revised World Health Organization classification

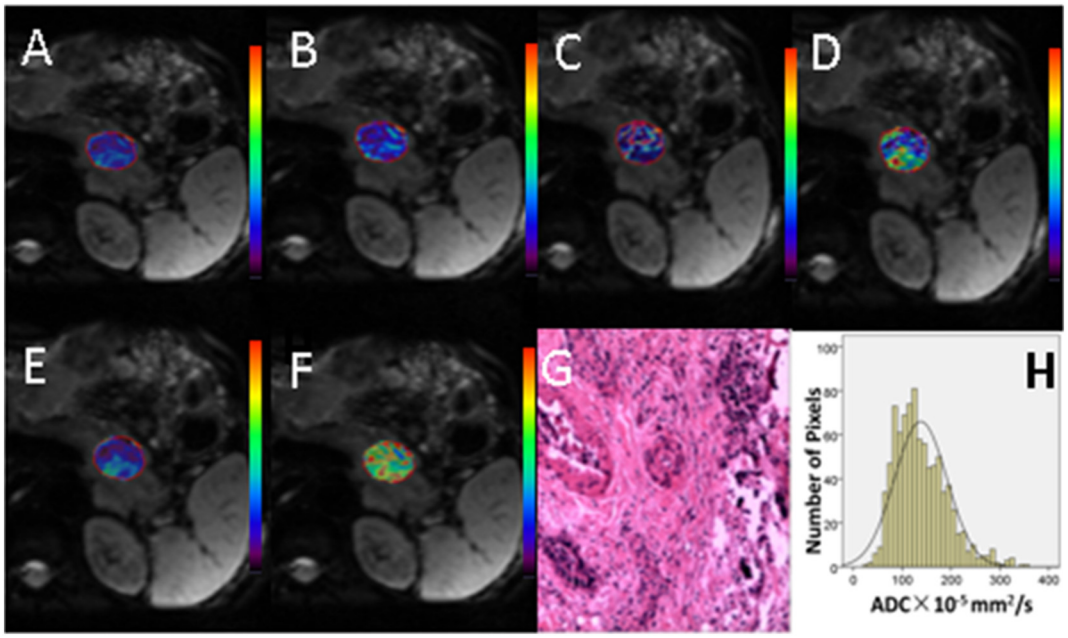

Fig. 3. Representative images of a 52-year-old man diagnosed with pancreatic ductal adenocarcinomas (PDAC).
A–F: pseudocolor maps of ADC, Dt, Dp, f, DDC, and α, respectively.
The mean ADC, Dt, Dp, f, DDC, and α values of the lesion were $135 \times 10^{-5}\,mm^2/s$, $99.06 \times 10^{-5}\,mm^2/s$, $628 \times 10^{-5}\,mm^2/s$, 167.6×10^{-3}, $114.5 \times 10^{-5}\,mm^2/s$, 747×10^{-3} respectively.
G: Histopathological examination showed that the tumor was a PDAC
(H&E image, original magnification, ×100).
H: The histogram of ADC map.

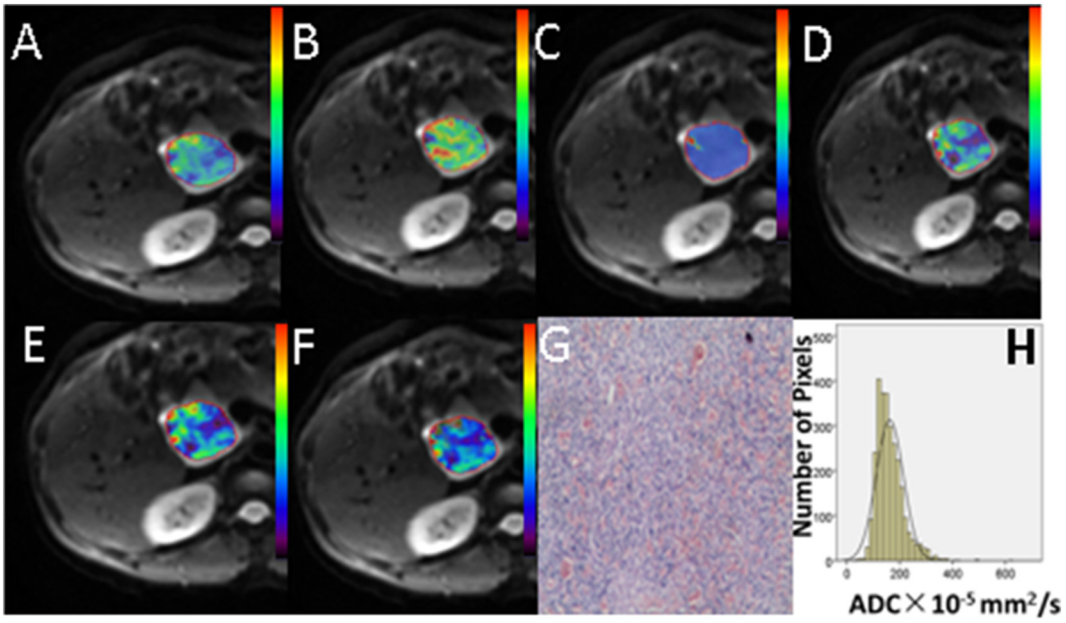

Fig. 4. Representative images of a 28-year-old woman diagnosed with pancreatic neuroendocrine tumors (pNET).
A–F: pseudo color maps of ADC, Dt, Dp, f, DDC, and α, respectively.
The mean ADC, Dt, Dp, f, DDC, and α values of the lesion were $187.52 \times 10^{-5}\,mm^2/s$, $122.56 \times 10^{-5}\,mm^2/s$, $862 \times 10^{-5}\,mm^2/s$, 217×10^{-3}, $170.41 \times 10^{-5}\,mm^2/s$, 738×10^{-3}, respectively.
G: Histopathological examination showed that the tumor was a pNET
(H&E image, original magnification, ×100).
H: The histogram of ADC map.

Table 4
Effectiveness of histogram parameters in discriminating pNET from PDAC.

Parameter	AUC	Cutoff value[a,b]	Sensitivity (%)	Specificity (%)	Youden index
ADC					
Mean	0.806(0.686–0.895)	218	88.1	65	0.531
Median	**0.846(0.757–0.940)**	**200**	**85.71**	**90**	**0.757**
10th percentile	0.801(0.680–0.891)	142	95.24	55	0.502
90th percentile	0.761(0.636–0.860)	250.9	54.76	90	0.448
Dt					
Mean	0.530(0.399–0.658)	132.56	51.43	80	0.314
Median	0.560(0.428–0.686)	118.5	57	70	0.274
10th percentile	0.526(0.395–0.654)	129	97.6	30	0.276
90th percentile	0.556(0.424–0.682)	250	97.62	35	0.326
Dp					
Mean	0.811(0.691–0.899)	653	50	100	0.500
Median	**0.877(0.769–0.947)**	**601**	**90.48**	**75**	**0.654**
10th percentile	0.857(0.744–0.933)	224	71.41	90	0.638
90th percentile	0.668(0.537–0.783)	751	35.71	100	0.357
f					
Mean	0.861(0.750–0.936)	209	95.24	70	0.652
Median	**0.919(0.821–0.973)**	**188**	**97.62**	**80**	**0.776**
10th percentile	0.837(0.721–0.919)	41	71.43	90	0.614
90th percentile	0.801(0.680–0.891)	461	90.48	65	0.528
DDC					
Mean	0.836(0.721–0.918)	167.17	80.95	80	0.610
Median	**0.858(0.774–0.950)**	**176**	**88.1**	**80**	**0.681**
10th percentile	0.693(0.563–0.804)	107.8	66.67	75	0.417
90th percentile	0.852(0.739–0.929)	239	66.67	95	0.617
α					
Mean	0.833(0.717–0.916)	766.6	85.71	85	0.707
Median	**0.864(0.753–0.938)**	**743**	**90.48**	**75**	**0.655**
10th percentile	0.714(0.585–0.822)	566	69.05	75	0.357
90th percentile	0.744(0.617–0.846)	997	78.57	70	0.486

95% confidence intervals were shown in parentheses. Best AUC results printed in bold.
PDAC = pancreatic ductal adenocarcinomas, pNET = pancreatic neuroendocrine tumors.
[a] Units of 10^{-5} mm^2/s for ADC, Dt, Dp and DDC.
[b] Units of 10^{-3} mm^2/s for f and a in terms of mean, median, 10th and 90th percentile.

Table 5
Comparison of area under the receiver operating characteristic curve values of DWI parameters.

Parameter	ADC-median	Dp-median	f-Median	DDC-median
Dp-median	0.617			
f-Median	0.224	0.473		
DDC-median	0.868	0.763	0.336	
α-Median	0.788	0.843	0.392	0.921

Data are *P* values.
$P < 0.05$ indicated that the difference was statistically significant.

criteria, 45% pNETs (9 of 20) were G1 tumors, 35% pNETs (7 of 20) were G2 tumors, and 20% pNETs (4 of 20) were G3 tumors.

4. Discussion

4.1. Monoexpontional DWI model

During our study, ADC derived from monoexponential DWI model was significantly lower in PDACs than the pNETs. Consistent with this study, Concia et al. [21] and Toshikazu Shindo [22] et al. had reported ADC value could help distinguish pNET of PDAC. Theoretically, the higher cell density, richer fibrous tissue and interstitial components in pancreatic cancer could result in the decrease of ADC value (5). However, the study conducted by Bohyun Kim [23] mentioned that PDAC had significantly higher mean ADC value than pNET and another study of Koung Mi Kang et al. [24] demonstrated that mean ADC value was not significant between PDAC and pNET. These different results may be due to the following reasons. First, the choice of b value was different. Second, the methods to measure ADC value were changed. For instance, previous studies always selected single-slice of the tumor as ROI. Nevertheless, this study used whole lesion to calculate DWI parameters. These contradictory results indicated that ADC value (monoexpontional DWI model) may have some limitations in the identification of PDAC and pNET.

4.2. IVIM DWI model

This paper showed that Dt values derived from IVIM DWI model were not helpful in differentiating PDAC and pNETs. Similar findings were reported by Shindo et al. [25] and Bohyun Kim et al. [23] Dt could minimize the effect of perfusion and represent the true water molecule diffusion situation. Therefore, the above studies suggested that the difference between PDAC and pNET cannot be manifested only by the degree of true water molecules diffusion.

Dp and f value derived from IVIM DWI model were associated with quantitative perfusion in pancreas. The study of Klau et al. [26] showed that Dp and f may be favorable markers to quantify pancreatic tumor micro vessels, moreover, f value ha d excellent correlation with micro vessel density (MVD). The current study showed that histogram metrics derived from Dp and f value were significantly lower in PDAC than pNET. Similarly, previous studies of Lemke et al. [27] and Re et al. [28] indicated that the mean Dp and f value in pancreatic cancer were markedly lower than normal tissue. A convincing explanation is that PDAC has lower capillary density in intercellular space than pNET due to higher cell density [29]. In addition, neovascularization in malignant tissue tend to be distorted and branched, which may contribute to the

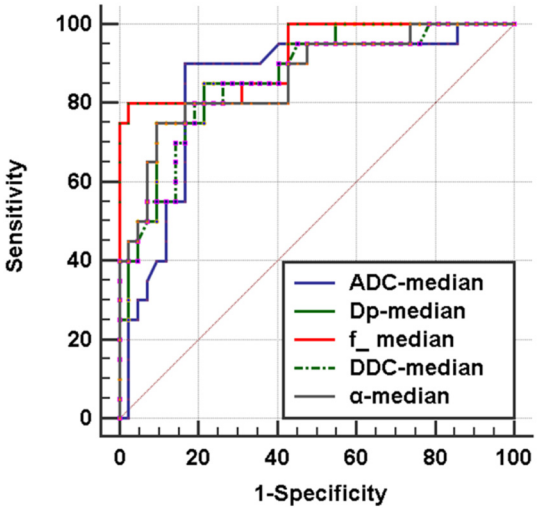

Fig. 5. ROC analysis of optimal histogram metric derived from every significant DWI parameter.
f-Median had the highest AUC of 0.919.

decrease of perfusion parameters in PDAC. Therefore, we believe that f and Dp values could be helpful in differentiating PDAC and pNET, especially in patients with contraindication to contrast agents or with atypical focal pancreatic lesions.

4.3. Stretched-exponential DWI model

To our knowledge, few papers applied stretched-exponential model to distinguish pancreatic tumors. However, some articles showed that the DDC and α value were significantly lower in gliomas than normal brain tissue [30,31], which suggested that DDC and α have a certain worth in the identification of benign and malignant organization. In this study, histogram metrics derived from α was significantly lower in pNET than PDAC. This result indicated that the organization heterogeneity of pNET is more complicated. It is possibly explained that pNET had higher cytoplasmic, microscopic hemorrhage and tortuous vascular hyperplasia [32,33]. In contrast, histogram metrics derived from DDC in PDAC was significantly lower than pNET. Hence the stretched-exponential model may be a potential new method for the identification of pancreatic tumors.

4.4. Histogram analysis

Whole-lesion analysis method can provide additional information and increase calculation accuracy compared with focusing on a limited tumor area [34]. During volumetric histogram analysis, median had greater AUC than mean and other percentiles for every significant DWI parameter, which suggested that it may be valuable to use the median in everyday clinical practice. In the comparisons of AUC, this study found the diagnostic efficacy of IVIM model (f and Dp) was higher than stretched-exponential model (DDC and α) and monoexponential model (ADC), although the AUC differences did not reach the statistical standard. Perhaps because the sample size is relatively small.

This study had several limitations. First, retrospective study may have the selection and verification biases. Second, the patient number was relatively limited, especially for pNET. Larger patient population was needed for further investigation. Third, due to the limited number of cases, this study did not research the neuroendocrine tumors pathological grade. Fourth, the correlations between f value and micro vessel had not been demonstrated because of lacking relative pathological parameters.

5. Conclusion

In summary, this paper indicated that volumetric histogram analysis via monoexponential and non-Gaussian diffusion models can be utilized to distinguish PDACs and pNETs. f-Median value derived from IVIM DWI model was more valuable parameter than ADC, Dp, DDC and α. It could improve the accuracy of diagnostic and contribute to determining an appropriate treatment strategy for pancreatic tumors.

Acknowledgements

This research was supported by the National Natural Science Foundation of China (grant numbers 81771801, 81701657, 81501447 and 81571642), and the Fundamental Research Funds for the Central Universities (grant number 2017KFYXJJ126).

References

[1] Dasari A, Shen C, Halperin D, Zhao B, Zhou S, Xu Y, et al. Trends in the incidence, prevalence, and survival outcomes in patients with neuroendocrine tumors in the United States. JAMA Oncol 2017;3(10):1335–42.
[2] Saif MW. Pancreatic neoplasm in 2011: an update. JOP 2011;12(4):316–21.
[3] Clancy TE. Surgical management of pancreatic neuroendocrine tumors. Hematol Oncol Clin North Am 2016;30(1):103–18.
[4] Chua TC, Yang TX, Gill AJ, Samra JS. Systematic review and meta-analysis of enucleation versus standardized resection for small pancreatic lesions. Ann Surg Oncol 2016;23(2):592–9.
[5] Liu JB, Baker MS. Surgical management of pancreatic neuroendocrine tumors. Surg Clin North Am 2016;96(6):1447–68.
[6] Pape UF, Jann H, Muller-Nordhorn J, Bockelbrink A, Berndt U, Willich SN, et al. Prognostic relevance of a novel TNM classification system for upper gastroenteropancreatic neuroendocrine tumors. Cancer 2008;113(2):256–65.
[7] Bednar F, Simeone DM. Recent advances in pancreatic surgery. Curr Opin Gastroenterol 2014;30(5):518–23.
[8] Lewis RB, Lattin Jr. GE, Paal E. Pancreatic endocrine tumors: radiologic-clinicopathologic correlation. Radiographics 2010;30(6):1445–64.
[9] Manfredi R, Bonatti M, Mantovani W, Graziani R, Segala D, Capelli P, et al. Non-hyperfunctioning neuroendocrine tumours of the pancreas: MR imaging appearance and correlation with their biological behaviour. Eur Radiol 2013;23(11):3029–39.
[10] Yang L, Krefting I, Gorovets A, Marzella L, Kaiser J, Boucher R, et al. Nephrogenic systemic fibrosis and class labeling of gadolinium-based contrast agents by the Food and Drug Administration. Radiology 2012;265(1):248–53.
[11] Taguchi N, Oda S, Utsunomiya D, Funama Y, Nakaura T, Imuta M, et al. Using 80 kVp on a 320-row scanner for hepatic multiphasic CT reduces the contrast dose by 50% in patients at risk for contrast-induced nephropathy. Eur Radiol 2017;27(2):812–20.
[12] Aronhime S, Calcagno C, Jajamovich GH, Dyvorne HA, Robson P, Dieterich D, et al. DCE-MRI of the liver: effect of linear and nonlinear conversions on hepatic perfusion quantification and reproducibility. J Magn Reson Imaging 2014;40(1):90–8.
[13] Ma C, Li YJ, Pan CS, Wang H, Wang J, Chen SY, et al. High resolution diffusion weighted magnetic resonance imaging of the pancreas using reduced field of view single-shot echo-planar imaging at 3 T. Magn Reson Imaging 2014;32(2):125–31.
[14] Zhang YD, Wang Q, Wu CJ, Wang XN, Zhang J, Liu H, et al. The histogram analysis of diffusion-weighted intravoxel incoherent motion (IVIM) imaging for differentiating the Gleason grade of prostate cancer. Eur Radiol 2015;25(4):994–1004.
[15] Federau C, Maeder P, O'Brien K, Browaeys P, Meuli R, Hagmann P. Quantitative measurement of brain perfusion with intravoxel incoherent motion MR imaging. Radiology 2012;265(3):874–81.
[16] Kim HS, Suh CH, Kim N, Choi CG, Kim SJ. Histogram analysis of intravoxel incoherent motion for differentiating recurrent tumor from treatment effect in patients with glioblastoma: initial clinical experience. Am J Neuroradiol 2014;35(3):490–7.
[17] Bennett KM, Schmainda KM, Bennett R, Rowe DB, Lu HB, Hyde JS. Characterization of continuously distributed cortical water diffusion rates with a stretched-exponential model. Magn Reson Med 2003;50(4):727–34.
[18] Li H, Liang L, Li A, Hu Y, Hu D, Li Z, et al. Monoexponential, biexponential, and stretched exponential diffusion-weighted imaging models: quantitative biomarkers for differentiating renal clear cell carcinoma and minimal fat angiomyolipoma. J Magn Reson Imaging 2017;46(1):240–7.
[19] Wang Y, Hu D, Yu H, Shen Y, Tang H, Kamel IR, et al. Comparison of the diagnostic value of monoexponential, biexponential, and stretched exponential diffusion-weighted MRI in differentiating tumor stage and histological grade of bladder cancer. Acad Radiol 2018. https://doi.org/10.1016/j.acra.2018.04.016. pii: S1076-6332(18)30199-5, [Epub ahead of print].
[20] Kang KM, Lee JM, Yoon JH, Kiefer B, Han JK, Choi BI. Intravoxel incoherent motion diffusion-weighted MR imaging for characterization of focal pancreatic lesions. Radiology 2014;270(2):444–53.
[21] Concia M, Sprinkart AM, Penner AH, Brossart P, Gieseke J, Schild HH, et al. Diffusion-weighted magnetic resonance imaging of the pancreas: diagnostic benefit from an intravoxel incoherent motion model-based 3 b-value analysis. Invest Radiol

2014;49(2):93–100.
[22] Yao XZ, Yun H, Zeng MS, Wang H, Sun F, Rao SX, et al. Evaluation of ADC measurements among solid pancreatic masses by respiratory-triggered diffusion-weighted MR imaging with inversion-recovery fat-suppression technique at 3.0 T. Magn Reson Imaging 2013;31(4):524–8.
[23] Kim B, Lee SS, Sung YS, Cheong H, Byun JH, Kim HJ, et al. Intravoxel incoherent motion diffusion-weighted imaging of the pancreas: characterization of benign and malignant pancreatic pathologies. J Magn Reson Imaging 2017;45(1):260–9.
[24] Donati OF, Mazaheri Y, Afaq A, Vargas HA, Zheng JT, Moskowitz CS, et al. Prostate cancer aggressiveness: assessment with whole-lesion histogram analysis of the apparent diffusion coefficient. Radiology 2014;271(1):143–52.
[25] Shindo T, Fukukura Y, Umanodan T, Takumi K, Hakamada H, Nakajo M, et al. Histogram analysis of apparent diffusion coefficient in differentiating pancreatic adenocarcinoma and neuroendocrine tumor. Medicine 2016;95(4).
[26] Klau M, Mayer P, Bergmann F, Maier-Hein K, Hase J, Hackert T, et al. Correlation of histological vessel characteristics and diffusion-weighted imaging intravoxel incoherent motion-derived parameters in pancreatic ductal adenocarcinomas and pancreatic neuroendocrine tumors. Invest Radiol 2015;50(11):792–7.
[27] Lemke A, Laun FB, Klauss M, Re TJ, Simon D, Delorme S, et al. Differentiation of pancreas carcinoma from healthy pancreatic tissue using multiple b-values comparison of apparent diffusion coefficient and intravoxel incoherent motion derived parameters. Invest Radiol 2009;44(12):769–75.
[28] Re TJ, Lemke A, Klauss M, Laun FB, Simon D, Grunberg K, et al. Enhancing pancreatic adenocarcinoma delineation in diffusion derived intravoxel incoherent motion f-maps through automatic vessel and duct segmentation. Magn Reson Med 2011;66(5):1327–32.
[29] Wang Y, Chen ZE, Nikolaidis P, McCarthy RJ, Merrick L, Sternick LA, et al. Diffusion-weighted magnetic resonance imaging of pancreatic adenocarcinomas: association with histopathology and tumor grade. J Magn Reson Imaging 2011;33(1):136–42.
[30] Bai Y, Lin YS, Tian J, Shi DP, Cheng JL, Haacke EM, et al. Grading of gliomas by using monoexponential, biexponential, and stretched exponential diffusion-weighted MR imaging and diffusion kurtosis MR imaging. Radiology 2016;278(2):496–504.
[31] Kwee TC, Galban CJ, Tsien C, Junck L, Sundgren PC, Ivancevic MK, et al. Intravoxel water diffusion heterogeneity imaging of human high-grade gliomas. NMR Biomed 2010;23(2):179–87.
[32] Reid MD, Balci S, Saka B, Adsay NV. Neuroendocrine tumors of the pancreas: current concepts and controversies. Endocr Pathol 2014;25(1):65–79.
[33] Singhi AD, Klimstra DS. Well-differentiated pancreatic neuroendocrine tumours (PanNETs) and poorly differentiated pancreatic neuroendocrine carcinomas (PanNECs): concepts, issues and a practical diagnostic approach to high-grade (G3) cases. Histopathology 2018;72(1):168–77.
[34] Lambregts DMJ, Beets GL, Maas M, Curvo-Semedo L, Kessels AGH, Thywissen T, et al. Tumour ADC measurements in rectal cancer: effect of ROI methods on ADC values and interobserver variability. Eur Radiol 2011;21(12):2567–74.